—Supporting Information—

Mobility of Soil-Biodegradable Nanoplastics in Unsaturated Porous Media Affected by Protein-Corona

Yingxue Yu[a], Odeta Qafoku[b], Libor Kovarik[b], Anton F. Astner[c], Douglas G. Hayes[c], Markus Flury[d,e,*]

[a] *Department of Environmental Science & Forestry, The Connecticut Agricultural Experiment Station, New Haven, CT 06511, USA*

[b] *Pacific Northwest National Laboratory, Richland, WA 99354, USA*

[c] *Department of Biosystems Engineering and Soil Science, The University of Tennessee, Knoxville, TN, 37996, USA*

[d] *Department of Crop & Soil Sciences, Puyallup Research & Extension Center, Washington State University, Puyallup, WA 98371, USA*

[e] *Department of Crop & Soil Sciences, Washington State University, Pullman, WA 99164, USA*

Number of pages: 18

Number of figures: 10

Number of tables: 2

*Corresponding author:

Markus Flury

E-mail: flury@wsu.edu

S1 Preparation of soil-biodegradable nanoplastics

Pristine soil-biodegradable nanoplastics with particle size < 450 nm were mechanically generated from a black soil-biodegradable plastic mulch film (29 ± 1.2 μm thick) made with PBAT (BioAgri, BioBag Americas, Dunedin, FL) Briefly, pieces (12 cm $\times$ 2 cm) of the mulch film were sequentially soaked in deionized water and liquid nitrogen, and then blended, milled, sieved, wet ground, and air-dried, producing pristine PBAT particles with size < 106 μm.[1] To obtain weathered PBAT particles, an aliquot (6 g) of the pristine PBAT particles (< 106 μm) was irradiated with a 1 kW xenon arc lamp (wavelength: 300–800 nm, 650 W m^{-2}) in an Atlas SunTest CPS+ solar simulator (Atlas Material Testing Technology LLC, Mount Prospect, IL) for 840 h. The 840-h exposure was chosen to mimic about 200 or 117 days of European mean solar exposure in Central and Southern Europe, respectively, assuming a yearly total of 1,000 and 17,000 kWh m^{-2} for Central and Southern Europe, respectively.[2] The plastic particles were placed into a Pyrex glass beaker (600 mL) covered with a glass Petri dish and were manually mixed every 24 h to ensure uniform weathering.

The pristine or the weathered PBAT particles with size < 106 μm were then suspended in deionized water, stirred on a magnetic plate for 5 h, sonicated for 10 min, and filtered through 0.45 μm filters (HAWP04700, MF-Millipore, MilliporeSigma, Burlington, MA). The filtrate was collected as the stock solution of pristine PBAT nanoplastics (200 mg L^{-1}, based on gravimetric analysis) or weathered PBAT nanoplastics (180 mg L^{-1}).

S2 Interaction energy calculations

We first calculated the total interaction energy (Φ_{total}) with the classical Derjaguin-Landau-Verwey-Overbeek (DLVO) theory for nanoplastics interacting with themselves and for nanoplastics interacting with the sand-water interface or the air-water interface.[3,4] Φ_{total} is the sum of the van der Waals energy (Φ_{vdw}) and the electrostatic double layer interaction energy (Φ_{dl}):

$$\Phi_{\text{total}}(h) = \Phi_{\text{vdw}}(h) + \Phi_{\text{dl}}(h) \tag{S1}$$

For nanoplastics interacting with themselves, Φ_{vdw} and Φ_{dl} are given as:

$$\Phi_{\text{vdw}}(h) = -\frac{A_{121}R}{12h}\left(1 + \frac{14h}{\lambda}\right)^{-1} \tag{S2}$$

$$\Phi_{\mathrm{dl}}(h) = 2\pi\varepsilon\varepsilon_0 R\phi^2 \ln[1 + \exp(-\kappa h)] \tag{S3}$$

where h is the distance between particles; A_{121} is the Hamaker constant for interactions between the particles, $A_{121} = (\sqrt{A_{11}} - \sqrt{A_{22}})^2$, where A_{11} is the Hamaker constant of nanoplastics, $A_{11} = 24\pi {\mathrm{d}_0}^2 \gamma_{\mathrm{P}}^{\mathrm{LW}}$, $\gamma_{\mathrm{P}}^{\mathrm{LW}}$ is the Lifshitz-van der Waals interfacial tension of nanoplastics, and A_{22} is the Hamaker constant of water, i.e., 3.7×10^{-20} J (ref[5]); R is the hydrodynamic radius of nanoplastics; λ is the characteristic length (100 nm); ε_0 is the permittivity in vacuum (8.85×10^{-12} C J^{-1} m^{-1}); ε is the relative dielectric permittivity of water (78.4); ϕ is the surface potential of nanoplastics, which is replaced by the ζ-potential; κ is the reciprocal Debye length, $\kappa = \sqrt{N_A e^2 \sum C_i z_i^2 / \varepsilon\varepsilon_0 k_B T}$, where N_A is the Avogadro number (6.02×10^{23} mol^{-1}), e is the electron charge (1.6×10^{-19} C), C_i is the molar concentration of the ith ion in the background electrolyte solution, z_i is the valence of ith ion, k_B is Boltzmann's constant (1.38×10^{-23} J K^{-1}), T is temperature (298 K).

For nanoplastics interacting with the sand-water interface or the air-water interface, Φ_{vdw} and Φ_{dl} are given as:

$$\Phi_{\mathrm{vdw}}(h) = -\frac{A_{123}R}{6h}\left(1 + \frac{14h}{\lambda}\right)^{-1} \tag{S4}$$

$$\Phi_{\mathrm{dl}}(h) = \pi\varepsilon\varepsilon_0 R(\phi_1^2 + \phi_2^2)\left\{\frac{2\phi_1\phi_2}{\phi_1^2 + \phi_2^2}\ln\left[\frac{1 + \exp\{(-\kappa h)\}}{1 - \exp\{(-\kappa h)\}}\right] + \ln[1 - \exp\{(-2\kappa h)\}]\right\} \tag{S5}$$

where A_{123} is the Hamaker constant for the particle interacting with the sand-water interface or the air-water interface, $A_{123} = (\sqrt{A_{11}} - \sqrt{A_{22}})(\sqrt{A_{33}} - \sqrt{A_{22}})$, where A_{33} is the Hamaker constant of the sand-water interface, i.e., 6.12×10^{-20} J,[6] or the air-water interface, i.e., 0 J; ϕ_1 and ϕ_2 are the ζ-potentials of nanoplastics and the sand-water interface (-45.2 ± 2.8 mV) or the air-water interface (-50 mV), respectively.[7]

In the extended DLVO theory, the hydrophobic interaction in the form of Lewis acid-base free energy of adhesion was included,[8] and Φ_{total} becomes the sum of van der Waals energy (Φ_{vdw}), electrostatic double layer interaction energy (Φ_{dl}), and Lewis acid-base interaction energy (Φ_{AB}):

$$\Phi_{\mathrm{total}}(h) = \Phi_{\mathrm{vdw}}(h) + \Phi_{\mathrm{dl}}(h) + \Phi_{\mathrm{AB}}(h) \tag{S6}$$

For nanoplastics interacting with themselves, Φ_{AB} is given as:

$$\Phi_{\mathrm{AB}}(h) = \pi R\lambda_{AB}\Delta\Phi_{\mathrm{d_0}}^{\mathrm{AB}} \exp\left(\frac{d_0 - h}{\lambda_{AB}}\right) \tag{S7}$$

where λ_{AB} is the water decay length for acid-base interactions (1 nm) (ref[9]); d_0 is the distance of closest approach and is assumed to be 0.157 nm (ref[10]); $\Delta\Phi_{\mathrm{d_0}}^{\mathrm{AB}}$ is the free energy adhesion at d_0 (ref[8]):

$$\Delta\Phi_{\mathrm{d_0}}^{\mathrm{AB}} = -4\left[\sqrt{\gamma_{\mathrm{P}}^{+}}\sqrt{\gamma_{\mathrm{P}}^{-}} + \sqrt{\gamma_{\mathrm{W}}^{+}}\sqrt{\gamma_{\mathrm{W}}^{-}} - \sqrt{\gamma_{\mathrm{P}}^{+}}\sqrt{\gamma_{\mathrm{W}}^{-}} - \sqrt{\gamma_{\mathrm{W}}^{+}}\sqrt{\gamma_{\mathrm{P}}^{-}}\right] \tag{S8}$$

where γ_{P} and γ_{W} is the surface energy of nanoplastics and water, respectively, and superscripts "+" and "−" denote the electron acceptor and the donor parameter of the surface, respectively.

For nanoplastics interacting with the sand-water interface or the air-water interface, Φ_{AB} is given as:

$$\Phi_{\mathrm{AB}}(h) = 2\pi R\lambda_{AB}\Delta\Phi_{\mathrm{d_0}}^{AB}\exp\left(\frac{d_0 - h}{\lambda_{AB}}\right) \tag{S9}$$

where $\Delta\Phi_{\mathrm{d_0}}^{\mathrm{AB}}$ is the free energy adhesion at d_0 (ref[11]):

$$\Delta\Phi_{\mathrm{d_0}}^{\mathrm{AB}} = 2\left[\sqrt{\gamma_{\mathrm{W}}^{+}}\left(\sqrt{\gamma_{\mathrm{P}}^{-}} + \sqrt{\gamma_{\mathrm{S}}^{-}} - \sqrt{\gamma_{\mathrm{W}}^{-}}\right) + \sqrt{\gamma_{\mathrm{W}}^{-}}\left(\sqrt{\gamma_{\mathrm{P}}^{+}} + \sqrt{\gamma_{\mathrm{S}}^{+}} - \sqrt{\gamma_{\mathrm{W}}^{+}}\right) - \sqrt{\gamma_{\mathrm{P}}^{-}\gamma_{\mathrm{S}}^{+}} - \sqrt{\gamma_{\mathrm{P}}^{+}\gamma_{\mathrm{S}}^{-}}\right] \tag{S10}$$

where γ_{S} is the surface energy of the sand or air surface. Values of γ_{W}^{+} and γ_{W}^{-} are 25.5 and 25.5 mJ m^{-2}, respectively. Values of γ_{S}^{+} and γ_{S}^{-} are 1.4 and 47.8 mJ m^{-2} for silica sand, and are 0 and 0 mJ m^{-2} for air. The γ_{P}^{+}, γ_{P}^{-} and $\gamma_{\mathrm{P}}^{\mathrm{LW}}$ of nanoplastics were derived from the Young-Dupré equation with contact angles for liquids of different polarity.[8] The contact angles of pristine PBAT, weathered PBAT, and PS-COOH nanoplastics were determined with the sessile drop method (DSA 100, Krüss, Hamburg, Germany) with water, formamide, and diiodomethane. For the pristine and weathered PBAT nanoplastics, a layer of the mulch particles was pressed onto a double-sided tape covered microscope slide.[12] For the PS-COOH nanoplastics, the suspension of PS-COOH nanoplastics was filtered through and deposited onto a 0.2 μm membrane (111106, Whatman Nuclepore Track-Etch Membrane) and the membrane was air-dried in a desiccator for 2 h and attached onto a microscope slide via double-sided tape. Then, a drop of the test liquid (2 μL) was placed onto the slide, and the contact angle was calculated based on the shape of the drop. The measured contact angles were 70 ± 3° (water), 47 ± 4° (formamide), and 43 ± 2° (diiodomethane) for the pristine PBAT particles, 61 ± 3° (water), 53 ± 2° (formamide), and 33 ± 4° (diiodomethane) for the weathered PBAT particles, and 80 ± 5° (water), 62 ± 3° (formamide), and 39 ± 4° (diiodomethane) for the PS-COOH nanoplastics.

In the modified DLVO theory, the steric repulsive energy was included for particle-particle and particle-collector interactions[13]:

$$\Phi_{\text{total}}(h) = \Phi_{\text{vdw}}(h) + \Phi_{\text{dl}}(h) + \Phi_{\text{steric}}(h) \tag{S11}$$

where $\Phi_{\text{steric}}(h)$ is the steric interaction energy:

$$\Phi_{\text{steric}}(h) = -\int_{\infty}^{h} F_{\text{steric}}(h)\ \mathrm{d}h \qquad (h \leq L) \tag{S12}$$

$$\Phi_{\text{steric}}(h) = 0 \qquad (h > L) \tag{S13}$$

$$F_{\text{steric}}(h) = 2\pi R \frac{k_B T}{s^3} \left\{ \frac{4L}{5} \left[\left(\frac{L}{h} \right)^{5/4} - 1 \right] + \frac{4L}{7} \left[\left(\frac{h}{L} \right)^{7/4} - 1 \right] \right\} \qquad (h \leq L) \tag{S14}$$

where $F_{\text{steric}}(h)$ is the steric force for particle-particle and particle-collector interactions, L is the thickness of protein-corona on nanoplastics, which was taken as 6.62 nm by considering a single layer of protein corona,[14,15] and s is the distance between the anchoring sites on the surface, which was taken as 5 nm.[14,15]

S3 Subsequent wetting after steady-state

To test whether PBAT nanoplastics could attach onto the air-water interface in the presence of LSZ, subsequent wetting was conducted at the end of the steady-state during transport experiments for the pristine and weathered PBAT nanoplastics at the low water saturation. A wetting front was induced in the sand column by increasing the inflow flux to 1.3 cm min^{-1}. The effluent was collected for ∼2 pore volumes and analyzed for PBAT with UV-vis spectrophotometry. Figure S9 shows the decrease of matric potentials of the column during the wetting phase.

S4 Transport of pristine PBAT nanoplastics in sand column previously flushed with LSZ

To test whether LSZ could attach onto the sand-water interfaces and thus provide additional attachment sites for the pristine PBAT nanoplastics, we first conducted transport experiment of LSZ at the low water saturation by injecting the LSZ suspension (10 mg L^{-1} LSZ in the background solution) for ∼1 pore volume and flushing the column with the background solution for ∼4 pore volumes. Then, we introduced the suspension of pristine PBAT

nanoplastics into the column for ∼1 pore volume followed with ∼4 pore volumes of the background solution. The LSZ concentration in the effluent was analyzed with the Bradford protein assay (Thermo Scientific Coomassie (Bradford) Protein Assay Kit, Thermo Fisher Scientific, Waltham, MA).

Literature Cited

(1) Astner, A. F.; Hayes, D. G.; O'Neill, H.; Evans, B. R.; Pingali, S. V.; Urban, V. S.; Young, T. M. Mechanical formation of micro- and nano-plastic materials for environmental studies in agricultural ecosystems. *Sci. Total Environ.* **2019**, *685*, 1097–1106.

(2) Solargis *Solar resource maps and GIS data for 200+ countries*; Solargis s.r.o.: Bratislavia, Slovakia, https://solargis.com/maps-and-gis-data/download/europe, accessed May 30, 2023, 2023.

(3) Gregory, J. Approximate expressions for retarded van der Waals interaction. *J. Colloid Interface Sci.* **1981**, *83*, 138–145.

(4) Hogg, R.; Healy, T. W.; Fuerstenau, D. W. Mutual coagulation of colloidal dispersions. *Trans. Faraday Soc.* **1966**, *62*, 1638–1651.

(5) Rijnaarts, H. H.; Norde, W.; Bouwer, E. J.; Lyklema, J.; Zehnder, A. J. B. Reversibility and mechanism of bacterial adhesion. *Colloids Surf. B: Biointerfaces* **1995**, *4*, 5–22.

(6) Bergendahl, J.; Grasso, D. Prediction of colloid detachment in a model porous media: Hydrodynamics. *Chem. Eng. Sci.* **2000**, *55*, 1523–1532.

(7) Yu, Y.; Elliott, M.; Chowdhury, I.; Flury, M. Transport mechanisms of motile and non-motile *Phytophthora cactorum* zoospores in unsaturated porous media. *Water Resour. Res.* **2021**, *57*, e2020WR028249, doi:10.1029/2020WR028249.

(8) van Oss, C. J. Long-range and short-range mechanisms of hydrophobic attraction and hydrophilic repulsion in specific and aspecific interactions. *J. Mol. Recognit.* **2003**, *16*, 177–190.

(9) Israelachvili, J. N. *Intermolecular and surface forces*, 2nd ed.; Academic Press: London, 1992.

(10) van Oss, C. J. *Interfacial forces in aqueous media*; CRC press: Boca Raton, Florida, 2006.

(11) Wang, D.; Zhang, W.; Hao, X.; Zhou, D. Transport of biochar particles in saturated granular media: effects of pyrolysis temperature and particle size. *Environ. Sci. Technol.* **2013**, *47*, 821–828.

(12) Shang, J.; Flury, M.; Harsh, J. B.; Zollars, R. L. Comparison of different methods to measure contact angles of soil colloids. *J. Colloid Interface Sci.* **2008**, *328*, 299–307.

(13) Petosa, A. R.; Jaisi, D. P.; Quevedo, I. R.; Elimelech, M.; Tufenkji, N. Aggregation and deposition of engineered nanomaterials in aquatic environments: Role of physicochemical interactions. *Environ. Sci. Technol.* **2010**, *44*, 6532–6549.

(14) Levak, M.; Burić, P.; Dutour Sikirić, M.; Domazet Jurašin, D.; Mikac, N.; Baćić, N.; Drexel, R.; Meier, F.; Jakšić, Ž.; Lyons, D. M. Effect of protein corona on silver nanoparticle stabilization and ion release kinetics in artificial seawater. *Environ. Sci. Technol.* **2017**, *51*, 1259–1266.

(15) Dong, Z.; Hou, Y.; Han, W.; Liu, M.; Wang, J.; Qiu, Y. Protein corona-mediated transport of nanoplastics in seawater-saturated porous media. *Water Res.* **2020**, *182*, 115978, doi:10.1016/j.watres.2020.115978.

Table S1. Experimental conditions of transport experiments.

Treatment	Replicate	S (%)	θ_v (cm^3 cm^{-3})	Q (mL min^{-1})	J_w (cm min^{-1})	v (cm min^{-1})	ψ (−cm H_2O)	M_{eff} (%)
Pristine PBAT	1	44	0.16	1.76	0.09	0.56	30	81
	2	44	0.16	1.76	0.09	0.56	30	80
	1	88	0.31	5.36	0.27	0.88	23	93
	2	88	0.31	5.36	0.27	0.88	23	95
Pristine PBAT + LSZ	1	49	0.18	1.73	0.09	0.49	30	51
	2	46	0.17	1.77	0.09	0.53	30	45
	1	86	0.31	5.48	0.28	0.90	23	69
	2	84	0.30	5.42	0.28	0.92	23	68
Pristine PBAT + BSA	1	45	0.16	1.70	0.09	0.54	30	87
	2	45	0.16	1.73	0.09	0.55	30	84
	1	85	0.30	5.36	0.27	0.91	23	94
	2	85	0.31	5.54	0.28	0.91	23	95
Weathered PBAT	1	45	0.16	1.70	0.09	0.54	30	78
	2	48	0.17	1.70	0.09	0.51	30	86
	1	83	0.30	5.48	0.28	0.93	23	98
	2	86	0.31	5.48	0.28	0.90	23	95
Weathered PBAT + LSZ	1	50	0.18	1.73	0.09	0.49	30	72
	2	50	0.18	1.70	0.09	0.48	30	77
	1	85	0.31	5.54	0.28	0.91	23	83
	2	84	0.30	5.42	0.28	0.92	23	85
Weathered PBAT + BSA	1	45	0.16	1.70	0.09	0.54	30	82
	2	47	0.17	1.74	0.09	0.52	30	82
	1	86	0.31	5.48	0.28	0.90	23	98
	2	82	0.29	5.41	0.28	0.95	23	92
PS-COOH	1	46	0.17	1.74	0.09	0.52	30	87
	2	49	0.18	1.77	0.09	0.50	30	88
	1	83	0.30	5.48	0.28	0.93	23	96
	2	84	0.30	5.48	0.28	0.93	23	98
PS-COOH + LSZ	1	48	0.17	1.70	0.09	0.51	30	0
	2	43	0.16	1.76	0.09	0.56	30	0
	1	83	0.30	5.48	0.28	0.93	23	0
	2	83	0.30	5.48	0.28	0.93	23	0
PS-COOH + BSA	1	44	0.16	1.73	0.09	0.55	30	87
	2	50	0.18	1.73	0.09	0.49	30	88
	1	84	0.30	5.42	0.28	0.92	23	99
	2	82	0.29	5.41	0.28	0.95	23	92

Abbreviations:

PBAT: polybutylene adipate co-terephthalate

LSZ: lysozyme

BSA: bovine serum albumin

PS-COOH: carboxylate-modified polystyrene

S: effective water saturation, defined as $S = \theta_v/\epsilon$, where θ_v is the volumetric water content, ϵ is the porosity (0.36 cm^3 cm^{-3}, determined from the bulk density of sand columns, i.e., 1.70 g cm^{-3})

Q: water flow rate

J_w: water flux (calculated by $J_w = Q/A$, where A is the cross section of the column)

v: pore water velocity (calculated by $v = J_w/\theta_v$)

ψ: matric potential

M_{eff}: percentage of nanoplastics recovered in the effluent.

Table S2. Average hydrodynamic diameter of nanoplastics determined from 60-min aggregation tests.

Nanoplastics	Proteins	Hydrodynamic diameter (nm)
Pristine PBAT	No protein	197 ± 12 (a)**
	10 mg L^{-1} LSZ	222 ± 3 (b)
	10 mg L^{-1} BSA	216 ± 20 (b)
Weathered PBAT	No protein	196 ± 11 (a)
	10 mg L^{-1} LSZ	253 ± 10 (b)
	10 mg L^{-1} BSA	215 ± 7 (c)
PS-COOH	No protein	222 ± 7 (a)
	10 mg L^{-1} LSZ	$2,216 \pm 658$ (b)
	10 mg L^{-1} BSA	230 ± 13 (c)

Measurements were done in a background solution consisted of 0.4 mM $NaHCO_3$ and 9.6 mM NaCl, pH $= 7.7 \pm 0.5$.

**Different letters in the parenthesis indicate significant differences between different treatments (Tukey's Multiple Comparison, $p = 0.01$). Data show mean $\pm$ standard deviation, $n = 4$.

Abbreviations: PBAT: polybutylene adipate co-terephthalate; LSZ: lysozyme; BSA: bovine serum albumin; PS-COOH: carboxylate-modified polystyrene

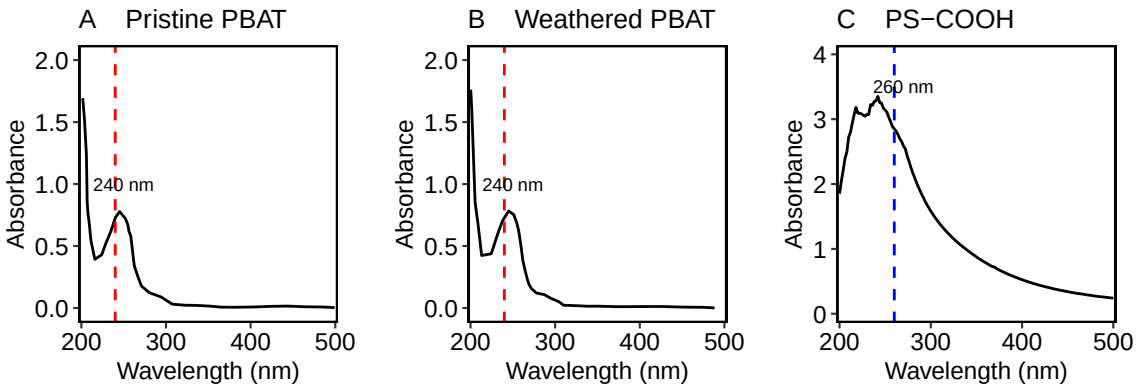

Figure S1. UV-vis spectra of (A) pristine PBAT (100 mg L^{-1}), (B) weathered PBAT (100 mg L^{-1}), and (C) PS-COOH (50 mg L^{-1}) nanoplastics in background solution (0.4 mM $NaHCO_3$ + 9.6 mM NaCl). Red and blue vertical dashed lines indicate the wavelengths chosen for concentration measurements for PBAT and PS-COOH nanoplastics. PBAT: polybutylene adipate co-terephthalate; PS-COOH: carboxylate-modified polystyrene.

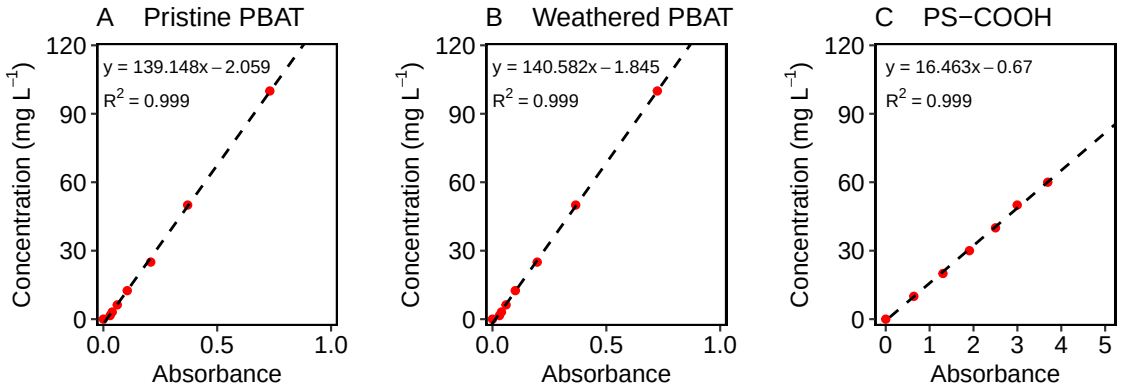

Figure S2. UV-vis absorbance vs concentrations calibration curves for (A) pristine PBAT at 240 nm wavelength, (B) weathered PBAT at 240 nm wavelength, and (C) PS-COOH at 260 nm wavelength in background solution (0.4 mM $NaHCO_3$ + 9.6 mM NaCl). PBAT: polybutylene adipate co-terephthalate; PS-COOH: carboxylate-modified polystyrene.

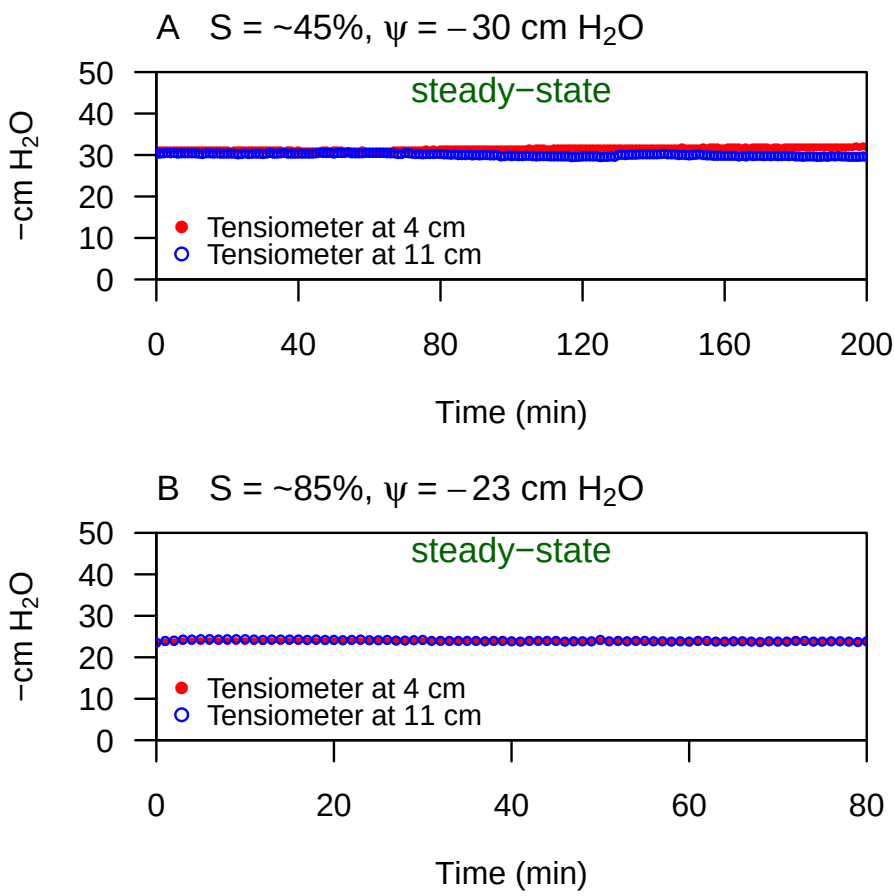

Figure S3. Representative water potentials measured with tensiometers during transport experiments. S: effective water saturation; ψ: matric potential applied by a hanging water tube at the bottom of the column. (A) Effective water saturation of 45%, (B) Effective water saturation of 85%.

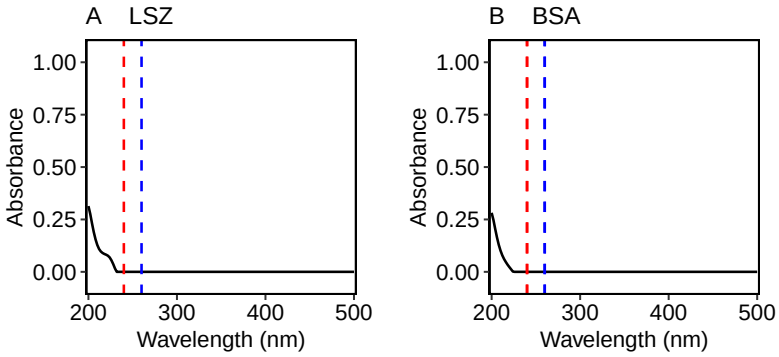

Figure S4. UV-vis spectra of (A) LSZ (10 mg L^{-1}) and (B) BSA (10 mg L^{-1}) in the background solution. Absorbance of LSZ at 240 nm (red line) and 260 nm (blue line) was zero, and absorbance of BSA at 240 nm (red line) and 260 nm (blue line) was zero. LSZ: lysozyme; BSA: bovine serum albumin.

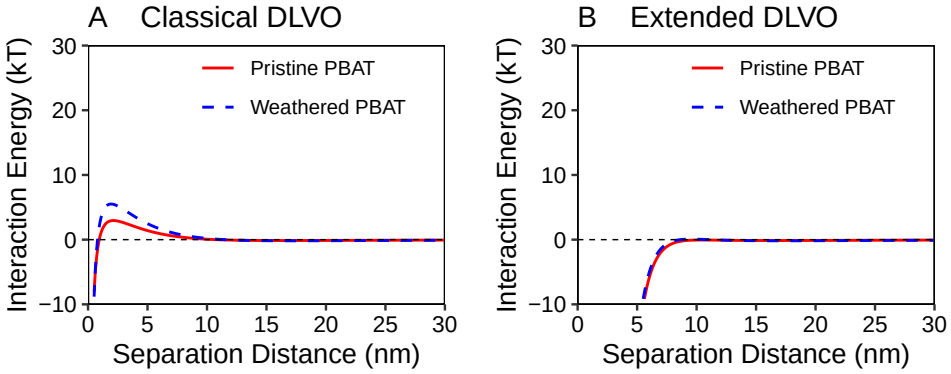

Figure S5. Total interaction energy between PBAT nanoplastics calculated with (A) the classical DLVO theory (Equations S1,S2,S3) and (B) the extended DLVO theory including the hydrophobic interaction in the form of Lewis acid-base free energy of adhesion (Equations S6,S2,S3,S7). PBAT: polybutylene adipate co-terephthalate.

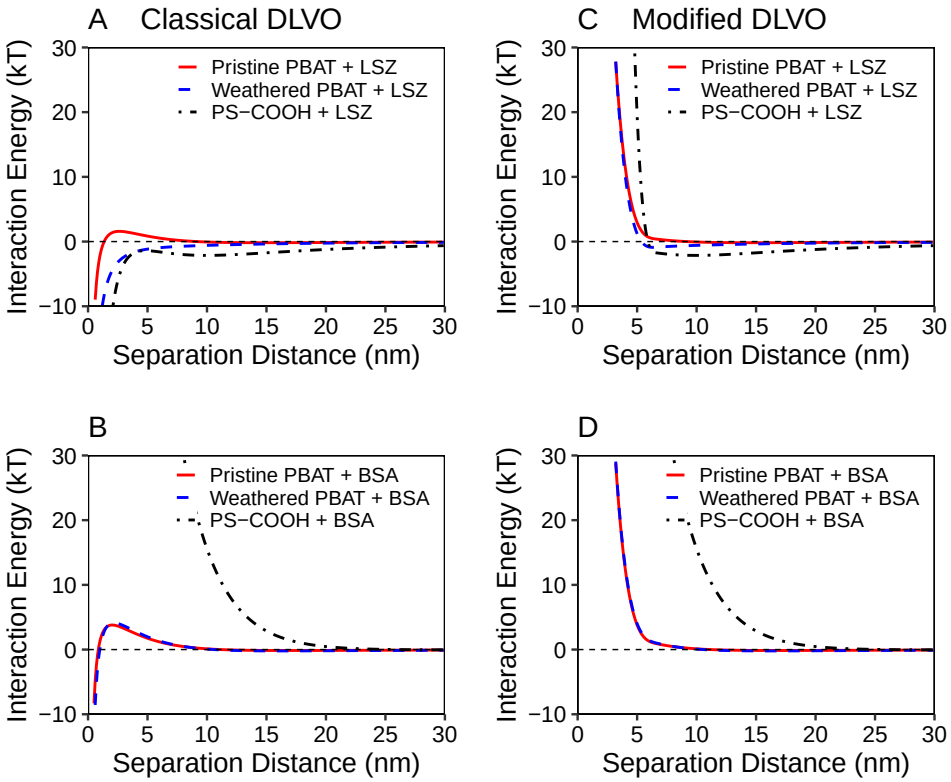

Figure S6. Total interaction energy between nanoplastics in the presence of proteins calculated with (A,B) the classical DLVO theory (Equations S1,S2,S3) and (C,D) the modified DLVO theory including the steric interaction (Equations S11,S2,S3,S12,S13,S14). PBAT: polybutylene adipate co-terephthalate; LSZ: lysozyme; BSA: bovine serum albumin; PS-COOH: carboxylate-modified polystyrene.

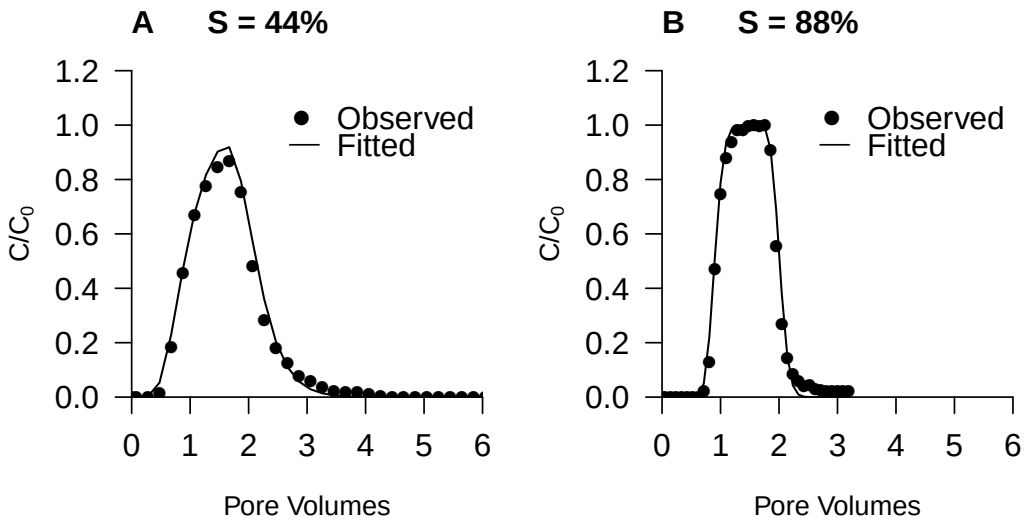

Figure S7. Representative tracer ($NaNO_3$) breakthrough curves at two different water saturations. S: effective water saturation; C: $NaNO_3$ concentration in the outflow; C_0: initial $NaNO_3$ concentration in the inflow; pore volume = outflow volume/($\theta_v \times$ column volume). Symbols are observed data and lines are fitted standard convection-dispersion model.

Nanoplastics interacting with sand-water interface Nanoplastics interacting with air-water interface

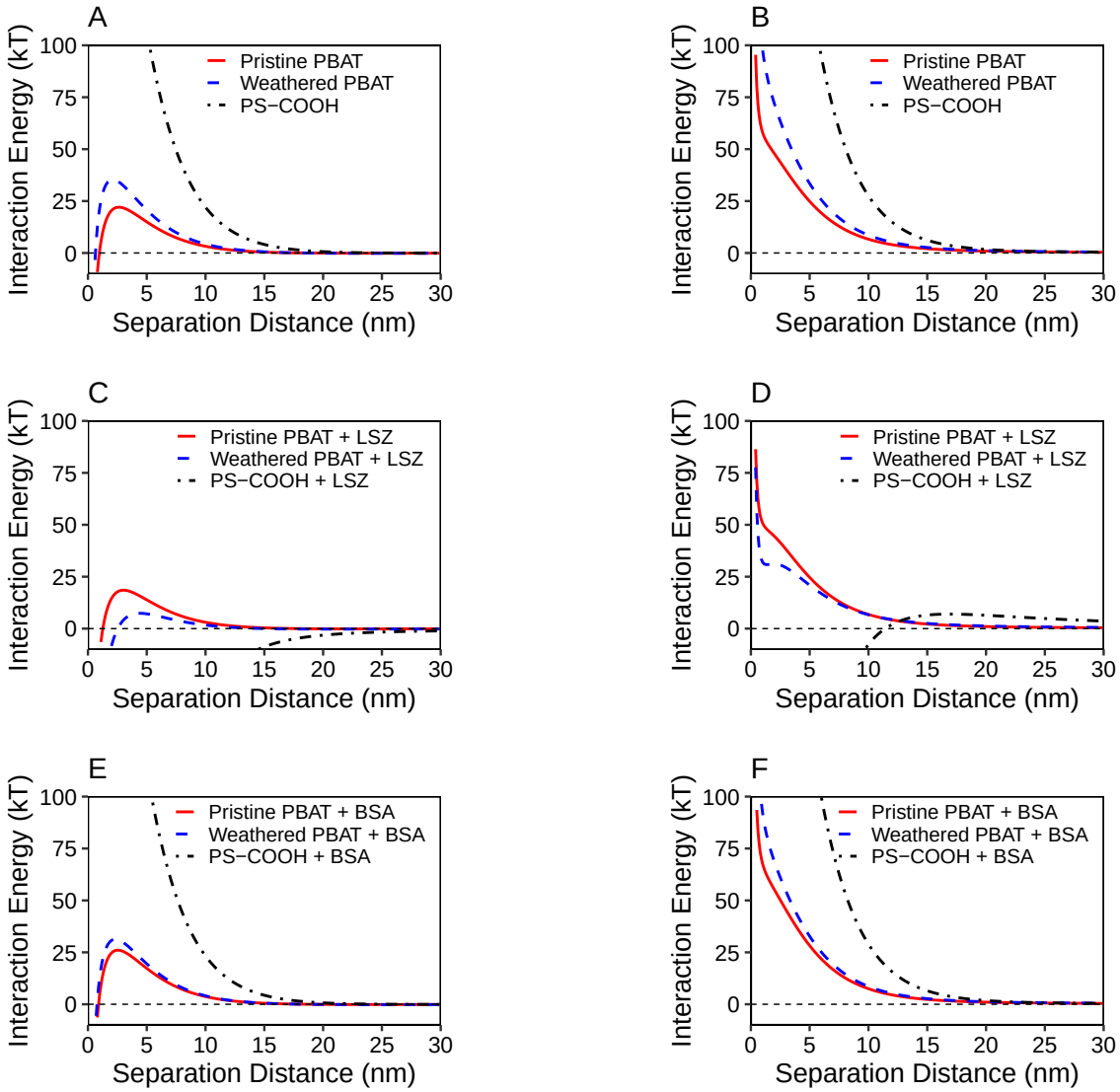

Figure S8. Total interaction energy for nanoplastics interacting with (A,C,E) the sand-water interface and (B,D,F) the air-water interface calculated with the classical DLVO theory (Equations S1,S4,S5) in the absence and presence of proteins. PBAT: polybutylene adipate co-terephthalate; PS-COOH: carboxylate-modified polystyrene; LSZ: lysozyme; BSA: bovine serum albumin.

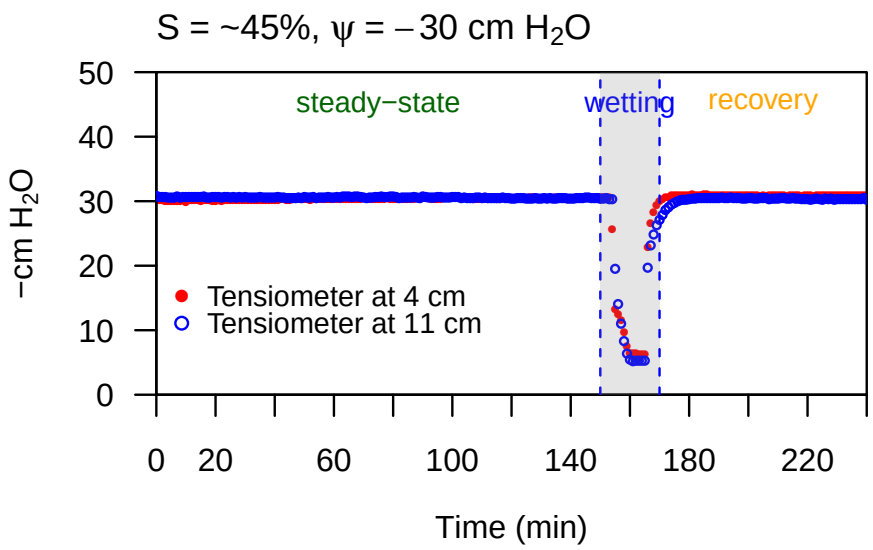

Figure S9. Water potentials measured with tensiometers during the wetting phase. S: effective water saturation; ψ: matric potential applied by a hanging water tube at the bottom of the column.

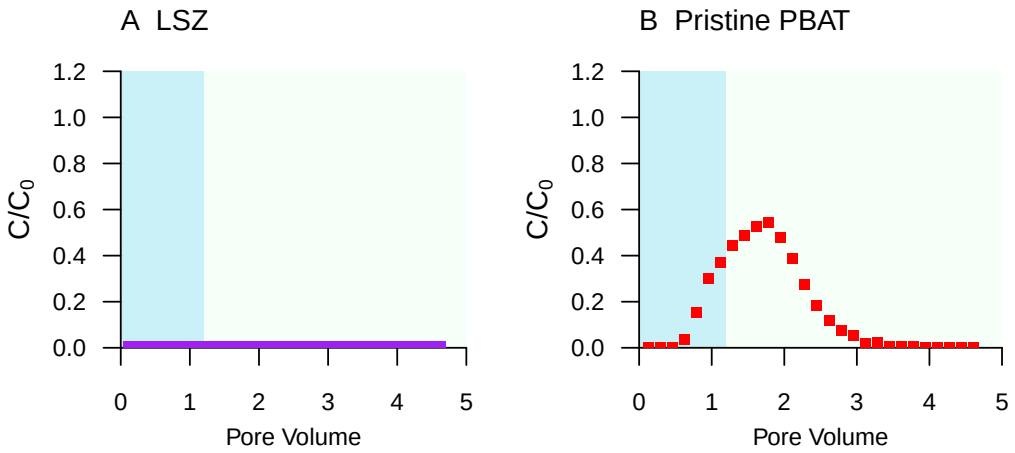

Figure S10. Breakthrough curves of LSZ and pristine PBAT nanoplastics. (A) Breakthrough curve of LSZ; (B) breakthrough curve of pristine PBAT nanoplastics in the sand column previously flushed with LSZ. The effective water saturation $S = 48\%$; C: nanoplastic concentration in the outflow; C_0: initial nanoplastic concentration in the inflow; pore volume = outflow volume/($\theta_v \times$ column volume). The blue and green shadings indicate the injection and elution phases of LSZ and pristine PBAT nanoplastics during the steady-state, respectively. PBAT: polybutylene adipate co-terephthalate; LSZ: lysozyme.